Photochemical & Photobiological Sciences (2022) 21:2153–2168
https://doi.org/10.1007/s43630-022-00285-1

ORIGINAL PAPERS

Spiro rhodamine-coumarin compact electron donor–acceptor dyads: synthesis and spin–orbit charge transfer intersystem crossing

Dongyi Liu[1] · Muhammad Imran[1] · Xiao Xiao[1] · Jianzhang Zhao[1]

Received: 14 April 2022 / Accepted: 8 August 2022 / Published online: 19 August 2022

Abstract

We prepared spiro rhodamine (RB)-coumarin (Cou) compact electron donor–acceptor dyads (**RB-Cou-CF$_3$** and **RB-Cou-CN**), to study the charge transfer (CT) and spin–orbit CT intersystem crossing (SOCT-ISC). The π-conjugation planes of the rhodamine and coumarin units in both dyads are in nearly orthogonal geometry (dihedral angle: 86.3°). CT state emission was observed for **RB-Cou-CF$_3$** (at 550 nm) and **RB-Cou-CN** (at 595 nm). Although the fluorescence of the pristine coumarin units (fluorescence quantum yields $\Phi_F = 59\%$) was quenched in the dyads ($\Phi_F = 0.5 \sim 1.1\%$ in *n*-hexane), the triplet state quantum yields of the dyads are also low (singlet oxygen quantum yield, $\Phi_\Delta = 2.3$–7.5% in *n*-hexane). Nanosecond transient absorption spectra show that the ^{3}Cou* state was formed, which shows a triplet state lifetime of 11–15.6 µs. The proposed photophysical path for the dyads is as follows: RB-^{1}Cou* → RB$^{+\bullet}$-Cou$^{-\bullet}$ → RB-^{3}Cou*. The low SOCT-ISC yield is attributed to the slightly lower charge-transfer state energy (1.94 eV in toluene) as compared to the ^{3}Cou* state energy (2.23 eV) and the shallow potential energy curve (PEC) at energy minima of the dyads. This work indicates that orthogonal conformation of donor–acceptor units is inadequate for achieving efficient SOCT-ISC. These results are useful for studying charge separation and intersystem crossing of electron donor/acceptor dyads.

Graphical abstract

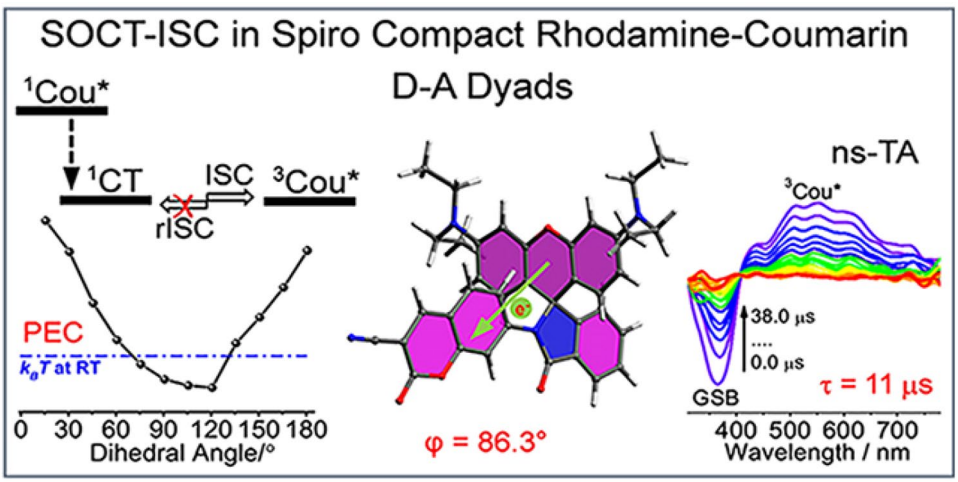

Dongyi Liu and Muhammad Imran contributed equally to this work.

✉ Jianzhang Zhao
zhaojzh@dlut.edu.cn

[1] State Key Laboratory of Fine Chemicals, School of Chemical Engineering, Dalian University of Technology, E-208 West Campus, 2 Ling Gong Road, Dalian 116024, People's Republic of China

1 Introduction

Triplet photosensitizers (PSs) are compounds that show strong absorption of visible light and efficient intersystem crossing (ISC) [1–3]. Triplet PSs are useful for the study of fundamental photochemistry, and the compounds have been

widely used in photocatalysis [4–6], photodynamic therapy [7–9], phosphorescence molecular probes [10–12], photovoltaics [13] and photon upconversion [14–17]. Most of the triplet PSs contain heavy atoms, such as Ru, Pt, Ir, I, or Br, to enhance the ISC [1, 2]. However, usage of these heavy atoms is a disadvantage due to the high cost and toxic nature of the triplet PSs. Therefore, it is highly desired to develop heavy atom-free triplet PSs [8]. However, from a photochemistry point of view, it is difficult to develop heavy atom-free triplet PSs because the ISC ability of the compounds becomes elusive without the heavy atom to enhance the spin–orbit coupling (SOC) [18]. Recently, a few approaches to design heavy atom-free triplet PSs have been reported, for instance, using exciton coupling [19, 20], electron spin converter [21–24], radical enhanced ISC (REISC) [25, 26], singlet fission [27], etc. Unfortunately, the triplet PSs based on these ISC mechanisms are usually synthetically demanding. For instance, the two identical chromophores of the triplet PSs based on exciton coupling have to be connected with rigid linkers and the two chromophores have to adopt a specific mutual orientation [19, 20, 28]. For this reason, a simple molecular structure motif for heavy atom-free triplet PSs is highly desired. Concerning this aspect, the charge recombination (CR)-induced ISC has attracted much attention recently, especially for the *compact* electron donor–acceptor (D-A) dyads, i.e. the donor and acceptor moieties are connected with short, simple linkers [29–31].

CR-induced ISC has been known for decades, especially for the molecular D-A systems mimicking natural photosynthesis centers [21, 32–35]. In those electron D-A dyads, the electron donor and acceptor are separated at large distances by the long and rigid linkers [36, 37]. The purpose of this molecular structure motif is to reduce the electronic coupling between the donor and acceptor and also the electron exchange energy of the electrons in the radical anion and cation; thus, the radical-pair ISC (RP-ISC) will occur. However, these electron D-A dyads are challenging to prepare from a synthesis point of view.

On the other hand, the *compact* electron D-A dyads are feasible to synthesize, but the electron exchange energy for the radical pairs in these dyads is large, as a result, the RP-ISC is inhibited [35]. However, given the electron donor and acceptor units in the compact dyads adopting orthogonal mutual orientation, then during CR, the molecular orbit angular momentum change offsets the electron spin angular momentum change of the ISC [38–43]. As a result, the CR-induced ISC will occur in these *orthogonal compact* electron D-A dyads, which is termed as spin–orbit charge transfer ISC (SOCT-ISC) [39–45].

Recently, the SOCT-ISC mechanism was reported in some compact electron D-A dyads, for instance, anthracene-phenothiazine [46], Bodipy-anthracene [47], Bodipy-phenothiazine [48], perylene-phenothiazine [49], perylenebisimide-carbazole [50], perylene-monoimide-phenothiazine [51, 52], naphthalimide-phenothiazine [53], etc. Moreover, the linkers in these compact orthogonal dyads are C–C or C–N single bond, which is able to rotate to some extent, although confirmation restriction was also imposed. Therefore, much room is left for designing novel molecular structural motifs to attain effective molecular conformation restriction and to study its effect on the SOCT-ISC efficiency.

Herein, we report novel *spiro* compact electron D-A dyads with lactam rhodamine as the electron donor and coumarin moiety as the electron acceptor [54, 55]. The *spiro* structure of the dyads is different from the previously reported compact D-A dyads showing the SOCT-ISC. Coumarin derivatives are well-known electron acceptors (reduction potential, $E_{Red} = -1.58$ to -1.74) V, vs Fc/Fc$^+$) with a high energy triplet state ($E_{T1} = 2.47$ to 2.65 eV) [56–59], which can be used in the construction of compact electron D-A dyads showing electron or charge transfer processes [59]. Coumarin was widely used in fluorescence probes, fluorescence bioimaging, and light-harvesting arrays [60, 61]. However, its application in the formation of triplet excited states in heavy atom-free organic compounds is rare. It was attached to a transition metal coordination center (Re(I), Ru(II), Ir(III), etc.) [62–64], to prepare triplet PSs. We synthesized two aminocoumarin derivatives containing two different electron-withdrawing groups (–CN, –CF_3) and linked them with rhodamine B by amidation reaction to obtain the target dyads **RB-Cou-CN** and **RB-Cou-CF$_3$** (Scheme 1). Various steady-state, time-resolved spectroscopic methods, electrochemical characterization, and density functional theory (DFT) computatiosn were used to unravel the photophysical properties. The formation of the triplet state of the dyads was investigated by nanosecond transient absorption (ns-TA) spectroscopy.

2 Experimental section

2.1 General methods

UV–vis absorption spectra were measured on an 8453 UV–vis spectrophotometer (Agilent Ltd., USA). Fluorescence emission spectra were recorded on an RF-5301PC spectrofluorometer (Shimadzu Ltd., Japan). C13534-11 UV-NIR absolute PL quantum yield spectrometer (Hamamatsu Ltd., Japan) was used to measure the absolute photoluminescence quantum yields. Luminescence lifetimes were measured on an OB920 photoluminescence lifetime spectrometer (Edinburgh Instruments, U.K.). For film preparation, the solution of **RB-Cou-CN** (1.0×10^{-4} mmol) was

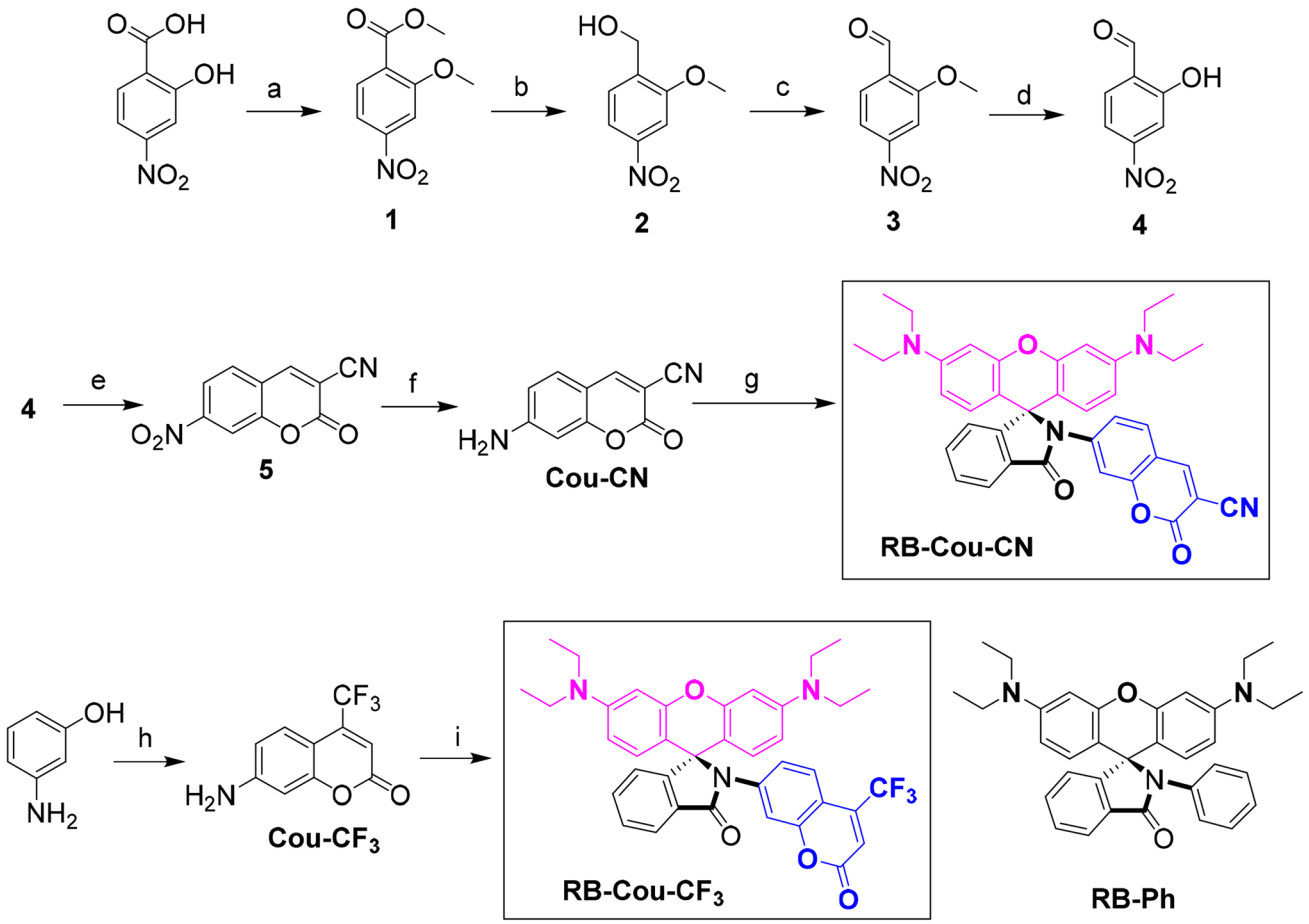

Scheme 1 Synthesis route of the spiro electron donor/acceptor dyads, reagents and conditions: **a** K_2CO_3, $(CH_3)_2SO_4$, acetone, reflux, 4 h, yield: 98%. **b** DIBAL–H (1 M in DCM), dry THF, 0 °C, 1 h, yield: 90%. **c** MnO_2, $CHCl_3$, reflux, 2.5 h, yield: 92%. **d** BBr_3, dry DCM, − 78 °C to rt, 5 h, yield: 92%. **e** Malononitrile, $NaHCO_3$ (aqueous, 0.1 M), rt, 2 h; HCl (con.), reflux, 1 h; yield: 92%. **f** TBAB, $SnCl_2{\cdot}H_2O$, 90 °C, 1 h, yield: 73%. **g** $POCl_3$, dry 1,2-dichloroethane, reflux, 4 h; **Cou-CN**, dry ACN, Et_3N, 55 °C, 30 h; yield: 13%. **h** *o*-aminophenol, $ZnCl_2$, EtOH, reflux, 8 h, yield: 10%. **i** $POCl_3$, dry 1,2-dichloroethane, reflux, 4 h; **Cou-CF$_3$**, ACN, Et_3N, 50 °C, 19 h; yield: 30%

injected into polyacrylate emulsion (0.5 mL), and then the transparent and flexible film was formed after drying in air.

2.1.1 Synthesis of RB-Cou-CN

Under N_2 atmosphere, rhodamine B (240 mg, 0.5 mmol) was dissolved in dry 1,2-dichloroethane (15 mL), then $POCl_3$ (0.5 mL) was added dropwise and the mixture was refluxed for 4 h. The solvent was evaporated under reduced pressure, then the crude product was dissolved in dry ACN (10 mL). Then **Cou-CN** (60 mg, 0.32 mmol) and Et_3N (0.7 mL) were added and the reaction mixture was stirred at 55 °C for 30 h. On completion of the reaction, the solvent was removed under reduced pressure and the crude product was purified by column chromatography (silica gel; DCM/ethyl acetate, 50:1, v/v). **RB-Cou-CN** was obtained as a yellow solid (26 mg, yield: 13%). ^{1}H NMR (400 MHz, $CDCl_3$, ppm) $\delta = 8.03$ (d, $J = 8.0$ Hz, 2H), 7.71 (s, 1H), 7.43 (dd, $J = 8.0$ Hz, $J = 8.0$ Hz, 4H), 7.09 (d, $J = 8.0$ Hz, 1H), 6.56 (s, 2H), 6.39 (s, 2H), 6.25 (s, 2H), 3.31–3.33 (m, 8H), 1.16 (t, $J = 16.0$ Hz, 12H); ^{13}C NMR ($CDCl_3$, 126 MHz): $\delta = 168.86$, 157.05, 154.82, 154.11, 152.44, 151.21, 149.06, 144.94, 134.15, 129.02, 128.41, 128.09, 127.75, 123.76, 123.67, 120.81, 113.94, 113.66, 110.76, 108.39, 105.62, 100.91, 98.11, 67.73, 44.34, 12.60; TOF–HRMS $[(C_{38}H_{34}N_4O_4)^+]$: calcd, $m/z = 611.2658$; found, $m/z = 611.2658$.

2.1.2 Synthesis of RB-Cou-CF$_3$

Under N_2 atmosphere, rhodamine B (240 mg, 0.18 mmol) was dissolved in dry DCM (5 mL) and then $POCl_3$ (0.5 mL) was added dropwise. The reaction mixture was refluxed and stirred for 4 h. The solvent was removed under reduced pressure; then crude product was dissolved in dry ACN (8 mL).

After that, a solution of **Cou-CF$_3$** (115 mg, 0.5 mmol) in dry ACN (8 mL) was added to the reaction mixture via syringe, and Et_3N (0.7 mL) was also added, then the mixture was refluxed for 19 h. On completion of the reaction, the solvent was removed under reduced pressure and the crude product was purified by column chromatography (silica gel; DCM as eluent). Compound **RB-Cou-CF$_3$** was obtained as a white-yellow solid (99 mg, yield: 30%). ^{1}H NMR (400 MHz, $CDCl_3$, ppm) $\delta = 7.99$ (d, $J = 8.0$ Hz, 1H), 7.43–7.52 (m, 4H), 7.09 (d, $J = 8.0$ Hz, 1H), 6.64 (s, 1H), 6.61 (s, 1H), 6.59 (s, 1H), 6.39 (s, 2H), 6.28 (d, $J = 8.0$ Hz, 2H), 3.30–3.35 (q, 8H), 1.16 (t, $J = 16.0$ Hz, 12H); ^{13}C NMR ($CDCl_3$, 126 MHz): $\delta = 168.57$, 154.38, 154.06, 152.56, 149.02, 133.81, 128.62, 128.31, 127.97, 125.06, 123.76, 123.62, 121.05, 114.45, 112.38, 110.45, 108.36,105.75, 98.07, 67.51, 44.33, 12.59. TOF–HRMS [($C_{38}H_{34}F_3N_3O_4 + H^+$)]: calcd, $m/z = 654.2580$; found, $m/z = 654.2579$.

2.2 Nanosecond time-resolved transient absorption spectroscopy

LP980 laser flash photolysis spectrometer (Edinburgh Instruments Ltd., UK) was used to record the ns-TA spectra of the compounds. An Opolette TM HE 355 UV nanosecond pulsed laser (OPOTEK, USA; pulse duration: 3–20 ns; typical laser power: 5 mJ per pulse; tuning: 210–2400 nm) was used as the excitation source, and xenon probe source was a 150 W ozone-free Xe arc lamp (pulsed frequency is up to 10 Hz). The transient signal was digitized with an oscilloscope (TDS 3012C, 100 MHz). Before measurements, all sample solutions were bubbled with N_2 for ca. 15 min. The recorded kinetic traces and transient spectra have been analyzed using L900 software.

2.3 DFT calculations

Density functional theory (DFT) was used to optimize the molecular structures of the compounds at the B3LYP and with range-separated functionals i.e. ωB97XD or CAM-B3LYP and 6-31G(d) basis set. The excitation energy or energy gaps between the S_0 state and the excited triplet states of the compounds were computed based on the optimal ground state geometry. All the calculations were performed with Gaussian 09W [65].

3 Results and discussion

3.1 Molecular structure design and synthesis scheme

Rhodamine is well known for the closed-form (lactam form) and the opened normal amide structural tautomerization [66]. In the opened form, the xanthene moiety is positively charged. However, rhodamine's closed-form (lactam structure) is neutral and acts as an electron donor. To our surprise, this structure was rarely used for the construction of electron donor–acceptor dyads for the study of electron transfer and charge separation [54, 67].

Recently we used this novel molecular structural motif to study charge transfer [54], although similar compounds were studied for aggregation-induced emission properties [55]. In this study, the rhodamine moiety acts as an electron donor and coumarin unit is an electron acceptor because the spiro lactam structure is beneficial for constructing rigid structures. The congested structure is beneficial for achieving an orthogonal orientation between the xanthene plane and the electron acceptor plane. Previously a cyclic peptide framework was used for the preparation of a rigid electron D-A dyad, but the synthesis was difficult, and the purpose was to produce a charge transfer state, not to attain a localized triplet state (^{3}LE) [68].

The synthesis of compounds **1**–**5**, **Cou-CN** and **Cou-CF$_3$** are based on the reported methods [69–74], The synthesis procedures along with molecular structures of the compounds are presented in Scheme 1. The molecular structures are fully verified with ^{1}H NMR, ^{13}C NMR and HR-MS spectra (see the Experimental Section and Supporting Information).

3.2 UV–vis absorption and luminescence emission spectra

The steady-state UV–vis absorption spectra of the compounds were studied (Fig. 1a). **Cou-CN** shows an absorption band centered at 390 nm, whereas **Cou-CF$_3$** shows an absorption band at 360 nm. For **RB-Cou-CN** and **RB-Cou-CF$_3$** dyads, due to the formation of amide structure, the electron-donating ability of the amino substitution on coumarin moiety is reduced. As a result, we observed a blue-shifted absorption band for **RB-Cou-CN** and **RB-Cou-CF$_3$** at 370 nm and 350 nm, respectively, as compared with the reference **Cou-CN** ($\lambda_{abs} = 390$ nm) and **Cou-CF$_3$** ($\lambda_{abs} = 360$ nm). It is known the rhodamine chromophore can undergo reversible closed form-opened form tautomerism in the presence of acid and base, respectively. In the presence of trifluoroacetic acid (TFA), a strong absorption band at 558 nm was observed for both **RB-Cou-CF$_3$** and **RB-Cou-CN**, indicating the stable nature of dyads in an acid-free environment (Fig. S14, ESI†).

The fluorescence of the compounds was studied (Fig. 1b,c). **Cou-CN** and **Cou-CF$_3$** show strong fluorescence (fluorescence quantum yields are $\Phi_F = 29\%$ and 59%, respectively, in *n*-hexane). In comparison, the fluorescence of the coumarin chromophore in the dyads is almost completely quenched (Fig. 1b), and the Φ_F are only 0.5–1.1% (in

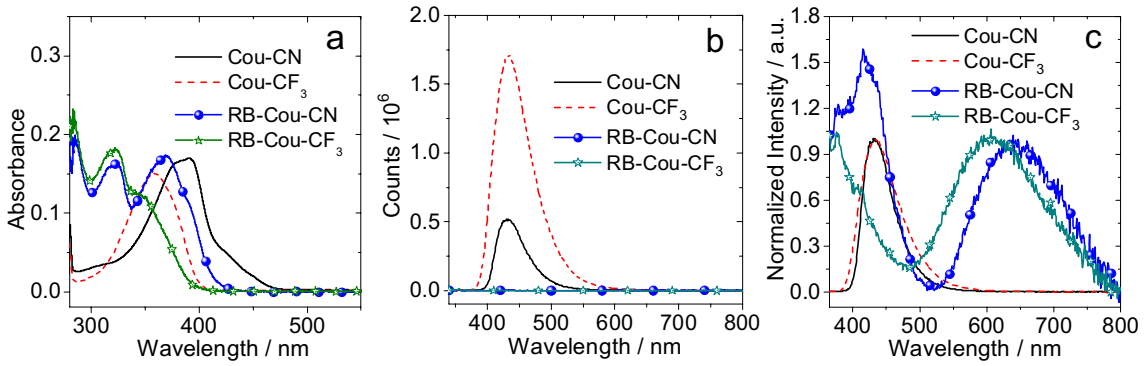

Fig. 1 **a** UV–vis absorption spectra of the compounds. **b** Fluorescence emission spectra of the compounds (optically-matched solutions were used, $A = 0.10$, $\lambda_{ex} = 320$ nm). **c** Normalized fluorescence emission spectra of the compounds. $c = 1.0 \times 10^{-5}$ M in toluene. 20 °C

Table 1 Photophysical parameters of the compounds

Compounds	λ_{abs} [a] (nm)	ε [b]	λ_{em} [c] (nm)	Φ_Δ [d] (%)	Φ_F [e] (%)	τ_F [f] (ns)	λ_P [g] (nm)	τ_P [h] (ms)	τ_T [i] (μs)
Cou-CN	390	1.70	430	[j]	29	2.8	[j]	[j]	[j]
Cou-CF$_3$	360	1.50	432	[j]	59	4.0	[j]	[j]	[j]
RB-Cou-CN	317	1.50	595	3.2	1.1	11.2	520/560	452	11.0
	370	2.06							
RB-Cou-CF$_3$	317	1.72	550	7.5	0.5	4.6	515/550	241	15.6
	350	1.41							

[a]Maximal UV–vis absorption wavelength, **Cou-CN** and **Cou-CF$_3$** in toluene, **RB-Cou-CN** and **RB-Cou-CF$_3$** in *n*-hexane, $c = 1.0 \times 10^{-5}$ M, 25 °C

[b]Molar absorption coefficient at absorption maxima, ε: 10^4 M^{-1} cm^{-1}

[c]Maximal emission wavelength, **Cou-CN** and **Cou-CF$_3$** in toluene, **RB-Cou-CN** and **RB-Cou-CF$_3$** in *n*-hexane, $\lambda_{ex} = 320$ nm, $A = 0.10$, 25 °C

[d]Singlet oxygen quantum yield in *n*-hexane, $Ru(bpy)_3[PF_6]_2$ was used as the standard compound ($\Phi_\Delta = 57\%$ in ACN)

[e]Absolute photo-luminescence quantum yield in *n*-hexane, error bar: ±0.1, $\lambda_{ex} = 360$ nm

[f]Luminescence lifetime, **Cou-CN** and **Cou-CF$_3$** in toluene, $c = 1.0 \times 10^{-5}$ M; **RB-Cou-CN** and **RB-Cou-CF$_3$** in deaerated *n*-hexane, $c = 2.0 \times 10^{-5}$ M; $\lambda_{ex} = 340$ nm

[g]Maximal phosphorescence wavelength in deaerated *n*-hexane, $c = 5.0 \times 10^{-5}$ M, $\lambda_{ex} = 340$ nm, at 77 K

[h]Phosphorescence lifetime in deaerated *n*-hexane, $c = 5.0 \times 10^{-5}$ M $\lambda_{ex} = 340$ nm, at 77 K

[i]Triplet state lifetimes, determined with ns-TA spectroscopy, in *n*-hexane

[j]Not observed

n-hexane, Table 1). This strong fluorescence quenching even in low polar solvents indicates that energy/electron transfer is feasible upon photoexcitation for both dyads. However, singlet energy transfer from the coumarin moiety to the lactam form of the rhodamine unit can be excluded due to the uphill feature of the singlet energy transfer. The most credible reason for fluorescence quenching is photoinduced electron transfer (PET) between rhodamine and coumarin moieties.

Notable here, besides the weak fluorescence bands of coumarin moiety (^{1}LE emission; locally excited) in **RB-Cou-CN** and **RB-Cou-CF$_3$**, a broad and weak emission band for the dyads centered at 550 nm and 595 nm was also observed in *n*-hexane, respectively (Fig. 1c and Fig. S15). The LE emission of **RB-Cou-CF$_3$** and **RB-Cou-CN** dyads is solvent polarity-independent. In contrast, the emission intensity at a longer wavelength sharply decreases and emission bands are red-shifted with increasing the solvent polarity (see Fig. S15, ESI†). Thus, the emission band at a longer wavelength is consistent with the solvent polarity-dependent charge transfer (CT) emission features [75]. On the basis of CT emission bands, we calculate ^{1}CT state energy in different solvents. For instance, the ^{1}CT state of **RB-Cou-CF$_3$** is estimated as 2.25 eV and 2.10 eV in *n*-hexane and toluene, respectively. Similarly, for **RB-Cou-CN**, the ^{1}CT energy in different solvents are 2.19 eV (in *n*-hexane) and 1.94 eV (in toluene).

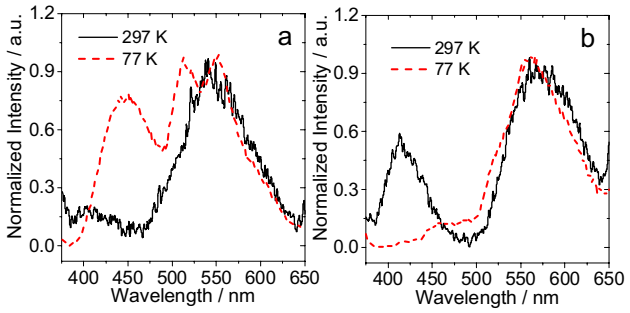

Fig. 2 Normalized luminescence spectra of the compounds. **a RB-Cou-CF$_3$** and **b RB-Cou-CN** at 297 K and 77 K, $\lambda_{ex}=340$ nm, in deaerated *n*-hexane, $c=5.0\times10^{-5}$ M

To obtain the triplet state energy of the dyads, we measured the luminescence spectra of the compounds at 77 K in deaerated *n*-hexane (Fig. 2, Fig. S16, ESI†). When the temperature decreased from 297 to 77 K, the emission intensity of both the dyads was enhanced, and the shape of the emission band changed. For instance, **RB-Cou-CF$_3$** shows three vibrational bands at ca. 450 nm, 515 nm and 550 nm (Fig. 2a). The lifetime of the 450 nm band is short, only 12.4 ns, while the other two bands have a long lifetime of 241 ms. For **RB-Cou-CN** (Fig. 2b), a broad emission band at about 570 nm was observed, but a shoulder band was also present at 520 nm. The lifetimes detected at 520 nm and 560 nm are 452 ms and 365 ms, respectively.

From these observations, we approximate ^{3}LE energy of **RB-Cou-CF$_3$** and **RB-Cou-CN** dyads as 2.23 eV and 2.17 eV, respectively. Moreover, the normalized luminescence spectra taken at 297 K and 77 K show that the ^{3}LE energy of **RB-Cou-CF$_3$** is close to the ^{1}CT state (2.25 eV in *n*-hexane). Although ^{1}CT/^{3}LE states share almost similar energy, the reverse ISC is nonefficient and thermally activated delayed fluorescence was not observed. This is confirmed by the fact that under deaerated conditions, fluorescence intensity/lifetimes of the dyads were not significantly increased (Fig. S17, ESI†). The same trend holds for **RB-Cou-CN**, which could be the reason for occurring the ISC in *n*-hexane. However, the energy gaps between ^{3}LE and ^{1}CT states increase with increased solvent polarity, and the ^{1}CT state lies much lower than ^{3}LE state. This mismatching of the states is obviously unfavorable for the efficient $^1\text{CT}\rightarrow{}^3$LE process of ISC.

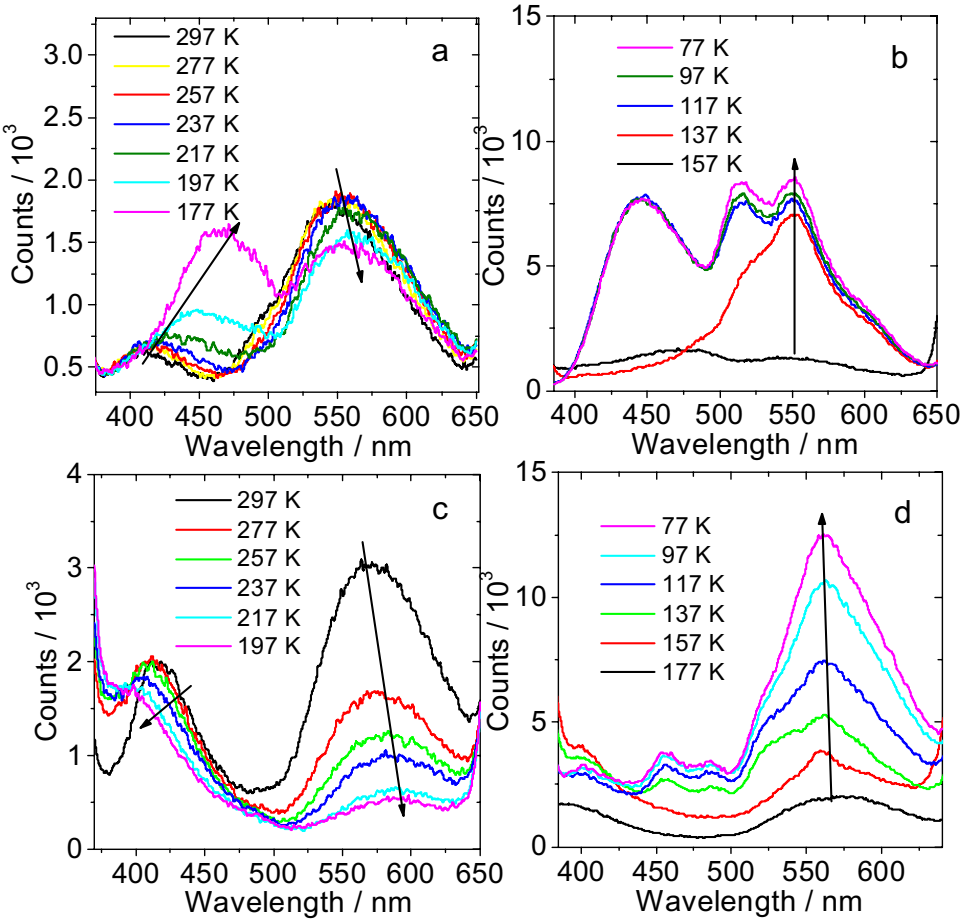

Fig. 3 Temperature-dependent luminescence spectra of **RB-Cou-CF$_3$**; **a** 297–177 K, **b** 157–77 K and **RB-Cou-CN**; **c** 297–197 K, **d** 177–77 K; $\lambda_{ex}=340$ nm, in deaerated *n*-hexane, $c=5.0\times10^{-5}$ M. Note: the melting point of *n*-hexane is 177 K

We, furthermore, measured the temperature-dependent (297–77 K) luminescence spectra of **RB-Cou-CF$_3$** and **RB-Cou-CN** dyads in deaerated *n*-hexane (Fig. 3). For **RB-Cou-CF$_3$** (Fig. 3a), with decreasing the temperature, the LE emission band at 410 nm sharply increases and red-shifted. In contrast, the CT emission band at about 550 nm slightly decreased and shifted bathochromically; therefore, it can be easily assigned to an intramolecular charge transfer (ICT) state [76]. It is noteworthy to mention that the reduced fluorescence intensity at lower temperatures is different from the normal fluorophores [18, 77]. When the temperature further decreased to 137 K (Fig. 3b), only one emission band centered at 550 nm was present, and its intensity drastically increased. From 117 to 77 K, the LE emission band in the range of 400–480 nm was raised again, while the band at 550 nm split into two peaks, and the lifetime was prolonged to a millisecond time scale. This can be assigned to the phosphorescence of coumarin moiety in the dyad. Similarly, for **RB-Cou-CN** (Fig. 3c), upon reducing the temperature, the LE emission decreased and blue-shifted, with the trend being opposite to that of **RB-Cou-CF$_3$**. Meanwhile, the CT emission band declined sharply and slightly red-shifted, hence it is assigned to a CT state [76]. Moreover, when the temperature dropped from 177 to 77 K (Fig. 3d), emission intensity at 570 nm gradually increased, and its lifetime was enhanced again due to the phosphorescence of coumarin moiety.

We also studied the luminescence properties of dyads in transparent/flexible polyacrylate film under different atmospheres and temperatures (Fig. 4 and Fig. S18, ESI†). For **RB-Cou-CN** under deaerated conditions, the emission band at 535 nm increased compared with emission measured in an aerated atmosphere (Fig. 4a). Luminescence lifetime is extended from 12.7 µs (Fig. S18, ESI†) to 6.0 ms (Fig. 4b). This emission band is similar to the phosphoresce band (measured at 77 K in deaerated *n*-hexane) and the CT band of **RB-Cou-CN** (Fig. 2b).

Since in aerated condition, this band is also long-lived. We conclude that the phosphorescence of **RB-Cou-CN** was observed under an aerated atmosphere when measured in film. Moreover, temperature-dependent (300–120 K) luminescence spectra of **RB-Cou-CN** in the film were also studied (Fig. 4c), and the luminescence intensity of 535 nm band increased with the decline of temperature.

The lifetime of this band is about 478.8 ms, probably the phosphorescence of coumarin moiety (Fig. 4d).

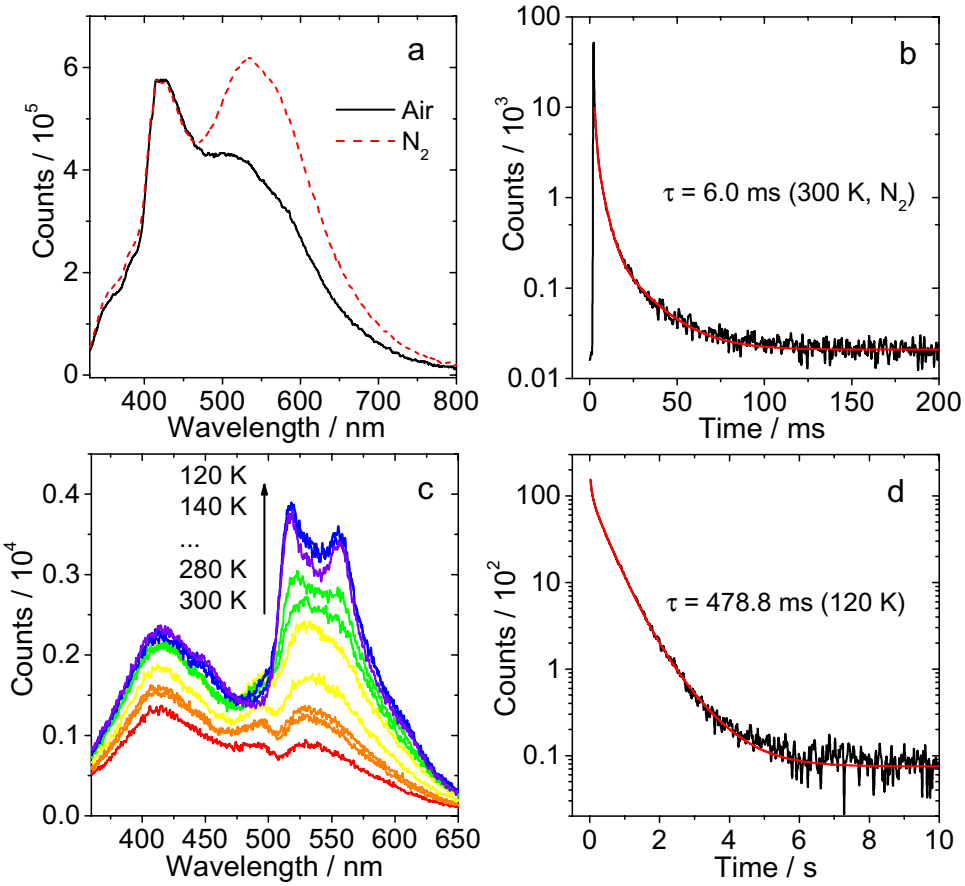

Fig. 4 Luminescence spectra of **RB-Cou-CN** in transparent/flexible film (polyacrylate emulsion). **a** Luminescence spectral comparison under aerated and deaerated conditions at 300 K and **b** decay trace at 300 K detected at 535 nm, in deaerated condition. **c** Temperature-dependent luminescence spectra and **d** decay trace at 120 K detected at 535 nm, in deaerated condition. $\lambda_{ex} = 340$ nm.

3.3 Electrochemical studies: cyclic voltammograms of the compounds

Cyclic voltammograms were recorded to study the electrochemical properties [21, 78]. In a reference *spiro* rhodamine with a phenyl attached at its amide position (**RB-Ph**), the two oxidation waves at + 0.52 V and + 0.67 V (vs. Fc/Fc^+) were observed, and there is no reduction wave within the potential range used in the electrochemical measurement [54, 67]. For **RB-Cou-CN** and **RB-Cou-CF$_3$** (Fig. 5), two oxidation waves at + 0.58 V and + 0.73 V (vs. Fc/Fc^+) were observed, the first oxidation wave is close to that of reference **RB-Ph**. An irreversible reduction wave at − 1.67 V was also observed for **RB-Cou-CN**. Similarly, an irreversible wave at − 1.85 eV was observed for **RB-Cou-CF$_3$**, which can be assigned to the coumarin unit. These results indicate that rhodamine unit acts as an electron donor and coumarin moiety as an electron acceptor in the dyads.

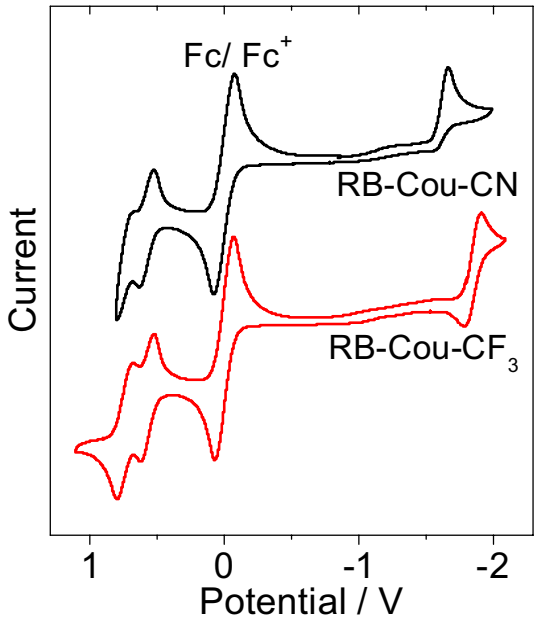

Fig. 5 Cyclic voltammograms of dyads. Conditions: in deaerated DCM containing 0.10 M Bu_4NPF_6 as supporting electrode, $Ag/AgNO_3$ as reference electrode, redox potential are versus Fc/Fc^+. Scan rates: 50 mV/s. $c = 1.0 \times 10^{-3}$ M. 20 °C

Gibbs free energy changes of the charge separation (ΔG_{CS}) and charge transfer states energy (E_{CT}) of **RB-Cou-CN** and **RB-Cou-CF$_3$** are calculated by using Rehm–Weller equations (Eqs. 1–3) [21], and the results are compiled in Table 2.

$$\Delta G_{CS} = e\left[E_{OX} - E_{RED}\right] - E_{00} + \Delta G_S \quad (1)$$

$$\Delta G_S = \frac{e^2}{4\pi\varepsilon_S\varepsilon_0 R_{CC}} - \frac{e^2}{8\pi\varepsilon_0}\left(\frac{1}{R_D} + \frac{1}{R_A}\right)\left(\frac{1}{\varepsilon_{REF}} - \frac{1}{\varepsilon_S}\right) \quad (2)$$

$$E_{CT} = e\left[E_{OX} - E_{RED}\right] + \Delta G_S \quad (3)$$

where ΔG_S is the static Coulombic energy which is described by Eq. (1). e = electric charge; E_{OX} = half-wave potential for one-electron transfer oxidation of the rhodamine unit; E_{RED} = half-wave potential for one-electron transfer reduction of the coumarin unit; E_{00} = excitation energy of that particular excited state; ε_S = static dielectric constant of the solvent; ε_0 = permittivity of free space; R_{CC} = center-to-center separation distance between an electron donor (rhodamine) and electron acceptor (coumarin), R_{CC} (**RB-Cou-CN**) = 5.38 Å and R_{CC} (**RB-Cou-CF$_3$**) = 5.37 Å are determined by DFT optimized geometry; R_D = radius of electron donor, R_A = radius of electron acceptor, ε_{REF} = static dielectric constant of the solvent used for the electrochemical studies [21].

For both dyads, ΔG_{CS} values are negative in all solvents (non-polar and polar), which shows that charge separation is thermodynamically allowed even in non-polar solvents such as *n*-hexane (Table 2). The conclusion agrees well with the luminescence emission spectra of the dyads that CT emission was observed in a non-polar solvent.

Table 2 Electrochemical parameters, Gibbs free energy changes of the charge separation (ΔG_{CS}) and charge transfer states energy levels (E_{CT}) of the compounds

Compounds	E_{OX} (V)	E_{RED} (V)	ΔG_{CS} (eV)/E_{CT} (eV)			
			HEX	TOL	DCM	ACN
RB-Ph[c]	+ 0.52, + 0.67	–[a]	–[b]	–[b]	–[b]	–[b]
RB-Cou-CN	+ 0.58, + 0.73	− 1.67	− 0.84/2.14	− 0.89/2.08	− 1.02/1.95	− 1.06/1.91
RB-Cou-CF_3	+ 0.57, + 0.73	− 1.85	− 0.90/2.31	− 0.97/2.26	− 1.16/2.12	− 1.20/2.08

Cyclic voltammetry in N_2-saturated DCM containing 0.10 M Bu_4NPF_6 solution, Pt electrode as the counter electrode, glassy carbon electrode as the working electrode, and $Ag/AgNO_3$ couple as the reference electrode, redox potentials are versus Fc/Fc^+

[a]Not observed

[b]Not applicable

[c]Values taken from reference [67]

3.4 Nanosecond transient absorption (ns-TA) spectroscopy: triplet state properties of the dyads

To study the formation of the triplet state of the dyads upon photoexcitation, nanosecond transient absorption (ns-TA) spectra of the compounds were measured in different solvents. For the reference compounds **Cou-CN** and **Cou-CF$_3$** upon excitation at 355 nm pulsed laser, no transient signals were observed in four representative deaerated solvents (HEX, TOL, DCM and ACN), hence ISC does not occur in the reference compounds and it is consistent with lack of singlet oxygen photosensitizing ability (Table S1, ESI†).

Upon photoexcitation of the dyads with 355 nm pulsed laser, however, transient absorption signals were detected for **RB-Cou-CN** and **RB-Cou-CF$_3$** in *n*-hexane (Fig. 6). For both the dyads, a ground state bleaching (GSB) band in the range of 300–400 nm and a broad excited state absorption (ESA) band in the range of 400–800 nm were observed (Fig. 6a, c). However, for **RB-Cou-CN**, a slightly different transient profile was observed upon laser excitation as compared with **RB-Cou-CF$_3$**, except for the GSB band centered at 360 nm. The ESA band is broader in a 400–800 nm range, while in the case of **RB-Cou-CF$_3$**, the ESA band is sharp and extended upto 750 nm. The lifetimes of the transient species were determined by monitoring the decay trances at ESA bands of **RB-Cou-CN** and **RB-Cou-CF$_3$** in deaerated *n*-hexane as 11.0 µs and 15.6 µs, respectively (Fig. 6b,d).

Moreover, when the solutions were exposed to air, the lifetimes of transient species significantly decreased (0.35–0.65 µs), whereas the ESA bands are similar to that observed in N_2-saturated solution (Fig. S19, ESI†). This result indicates that the transient species is O_2-sensitive and it could be LE triplet state; otherwise, the ESA profile will change under aerated conditions because the radical anion species can be easily quenched by O_2 [79]. Furthermore, the coumarin radical anion absorption should appear around 600 nm, but this is not the case detected [59]. The typical triplet ESA absorption range of coumarin moiety is from 450 to 800 nm [80–82], thus, we conclude that the ESA bands observed in **RB-Cou-CN** and **RB-Cou-CF$_3$** dyads can be ascribed to the $T_1 \rightarrow T_n$ transition of coumarin triplet state (^{3}Cou*). This is also in agreement with the DFT predictions, the triplet state spin density of the dyads is localized on the coumarin moiety (see the next section), further indicating that the final excited states of **RB-Cou-CN** and **RB-Cou-CF$_3$** in *n*-hexane should be ^{3}Cou*.

To study the effect of solvent polarity on ISC efficiency of dyads, ns-TA spectra were measured in deaerated TOL, DCM and ACN solvents, however, no triplet signals were detected. This could be due to the mismatching of ^{1}CT and

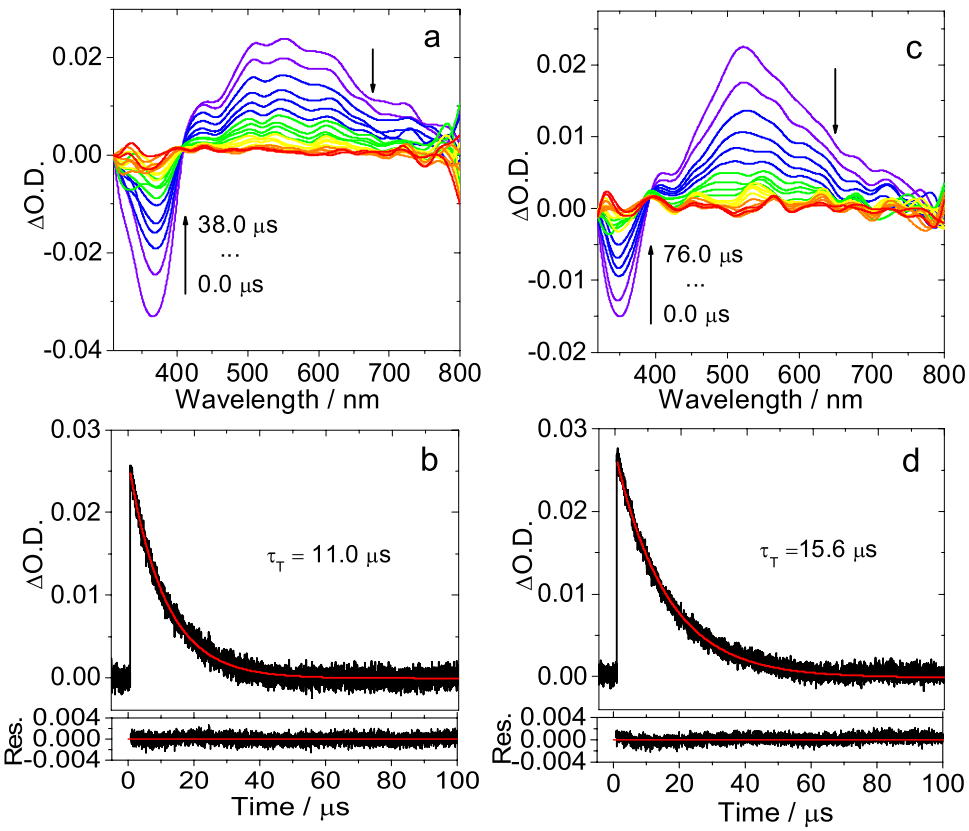

Fig. 6 **a** Nanosecond transient absorption spectra of **RB-Cou-CN** and **b** the decay trace at 560 nm. **c** Transient absorption spectra of **RB-Cou-CF$_3$** and **d** the decay traces at 520 nm. Excited with nanosecond pulsed laser, $\lambda_{ex} = 355$ nm, $c = 2.0 \times 10^{-5}$ M in deaerated *n*-hexane. 20 °C

^{3}LE states in different polarity solvents. For instance, the energy of ^{1}CT state (estimated by the onset CT emission band in TOL) of **RB-Cou-CF$_3$** is 2.07 eV, which is lower than that of the ^{3}Cou state (T_1 = 2.23 eV). Similarly, in ACN the ^{1}CT state could be lower than the ^{1}CT state in TOL and lies below the ^{3}LE state, and the same trend holds for **RB-Cou-CN**. In polar solvents, the CT state is non-emissive, and the CT state directly decayed to the ground state via CR.

3.5 Density functional theory: geometry optimization, potential energy surfaces and spin density distribution

To provide insight into the molecule structures and the photophysical property of the dyads, DFT calculations were used to optimize the molecular geometries of the compounds (Fig. 7). The optimized ground state conformations of **RB-Cou-CN** and **RB-Cou-CF$_3$** show that the dihedral angle between the xanthene and the coumarin planes for both dyads is 86.3°, which is beneficial for SOCT-ISC [39, 40, 42]. Moreover, the π-conjugation framework of two dyads is separated by three σ-bonds,

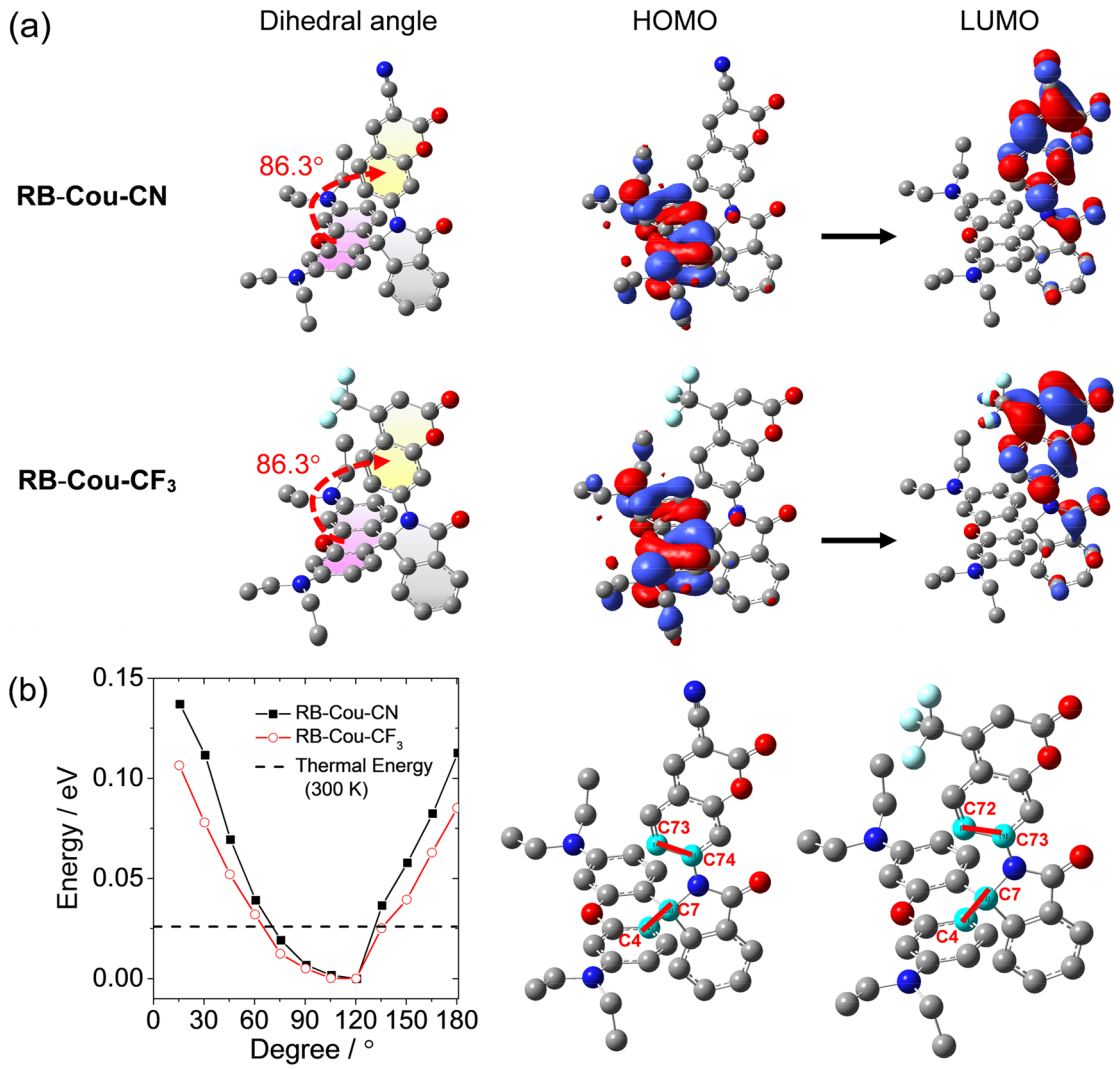

Fig. 7 **a** Optimized ground state conformations, HOMO and LUMO of **RB-Cou-CN** and **RB-Cou-CF$_3$**, isovalue = 0.03; the yellow and purple color sheets show the planes of the coumarin and the rhodamine moieties, respectively. **b** Ground state potential energy curves of **RB-Cou-CN** and **RB-Cou-CF$_3$**, as a function of the rotational dihedral angle of the selected atoms; the thermal energy (k_BT = 0.026 eV) at 300 K is indicated by a dashed line. All the calculations were based on the DFT (B3LYP/6–31G(d)) level with Gaussian 09 in vacuum. Hydrogen atoms are omitted for clarity

thus weak electronic coupling between the donor and acceptor is expected.

In addition, to investigate the electron transfer in **RB-Cou-CN** and **RB-Cou-CF$_3$** dyads, the distribution of frontier molecular orbitals, highest occupied molecular orbital (HOMO) and lowest unoccupied molecular orbital (LUMO) were studied (Fig. 7a). HOMO and LUMO are localized on xanthene and coumarin moieties, respectively, indicating the possibility of PET. The ground state potential energy curves (PECs) of **RB-Cou-CN** and **RB-Cou-CF$_3$** dyads against the torsion of the acceptor moiety about the linker are shown in Fig. 7b. The PECs generated by rotation about C − C bond of the selected atoms (**RB-Cou-CN**: ∠C4–C7–C74–C73, **RB-Cou-CF$_3$**: ∠C4–C7–C73–C72; the xanthene plane was fixed and the coumarin plane was rotating around the C–C bond of the dyads in the calculations) are shallow, and the energy barriers are small (< 0.15 eV) when the angles vary from 0° to 180°.

This indicates that only limited conformational restriction is applied. However, below the thermal energy range (k_BT = 0.026 eV, T = 300 K), the dihedral angles of the dyads can easily vary from 70° to 130°. According to previously reported bodipy-anthracene dyads with high singlet oxygen quantum yields, the PEC was steep and the energy barrier was much larger than the thermal energy at room temperature. Therefore, it was easy to be restricted to orthogonal conformation for those dyads [83]. However, for other bodipy-anthracene dyads with low singlet oxygen quantum yields, the PEC was shallower and the energy barrier was much smaller (< 0.4 eV), which can relax the geometry constrain [83]. In our case, the dihedral angles of **RB-Cou-CN** and **RB-Cou-CF$_3$** dyads are flexible and PECs are shallow, which are detrimental to attaining efficient SOCT-ISC. A significant deviation from the orthogonal geometry can lower triplet quantum yield, which could be the reason for the low singlet oxygen quantum yields of dyads.

The electron spin density distribution of the optimized triplet state geometry, radical anion and radical cation of the dyads are presented in Fig. 8. Spin unpaired electrons of the triplet state are mainly localized on coumarin moiety in both **RB-Cou-CN** and **RB-Cou-CF$_3$**, which is supported by the fact that the triplet state signal of coumarin was observed in the ns-TA spectra. The spin density in ACN is also calculated (Fig. S20, ESI†), the triplet spin density of **RB-Cou-CF$_3$** was still localized on the coumarin units, however, the triplet spin density of **RB-Cou-CN** was delocalized to rhodamine unit. Moreover, for both the dyads, the spin densities of the radical anion and radical cation are localized on the coumarin and xanthene moieties (Fig. 8), respectively. These computational results are also supported by an electrochemical study, further representing that the xanthene moiety acts as the electron donor and the coumarin unit as the electron acceptor in the PET process. Moreover, we also optimized and compared the DFT results obtained by B3LYP and using

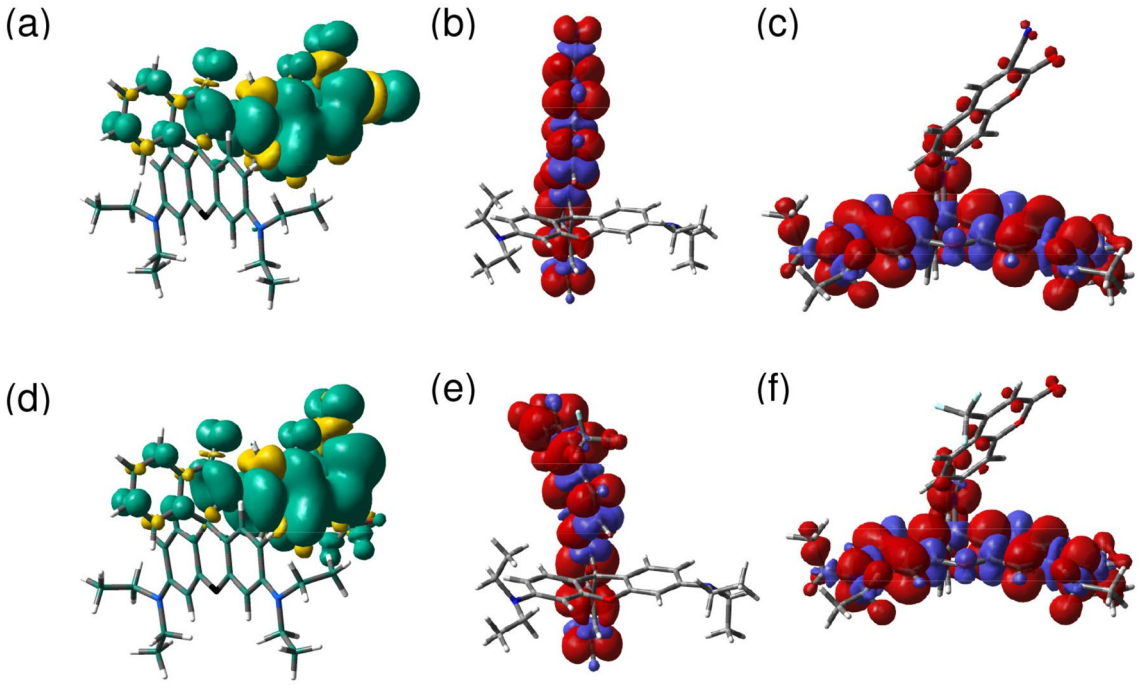

Fig. 8 Spin density distributions of **RB-Cou-CN** (upper panel) and **RB-Cou-CF$_3$** (lower panel) at the optimized (**a**, **d**) triplet state, (**b**, **e**) radical anion, and (**c**, **f**) radical cation geometries (isovalues are 0.0004) in cyclohexane. All the calculations were based on the DFT (B3LYP/6–31G(d)) level with Gaussian 09

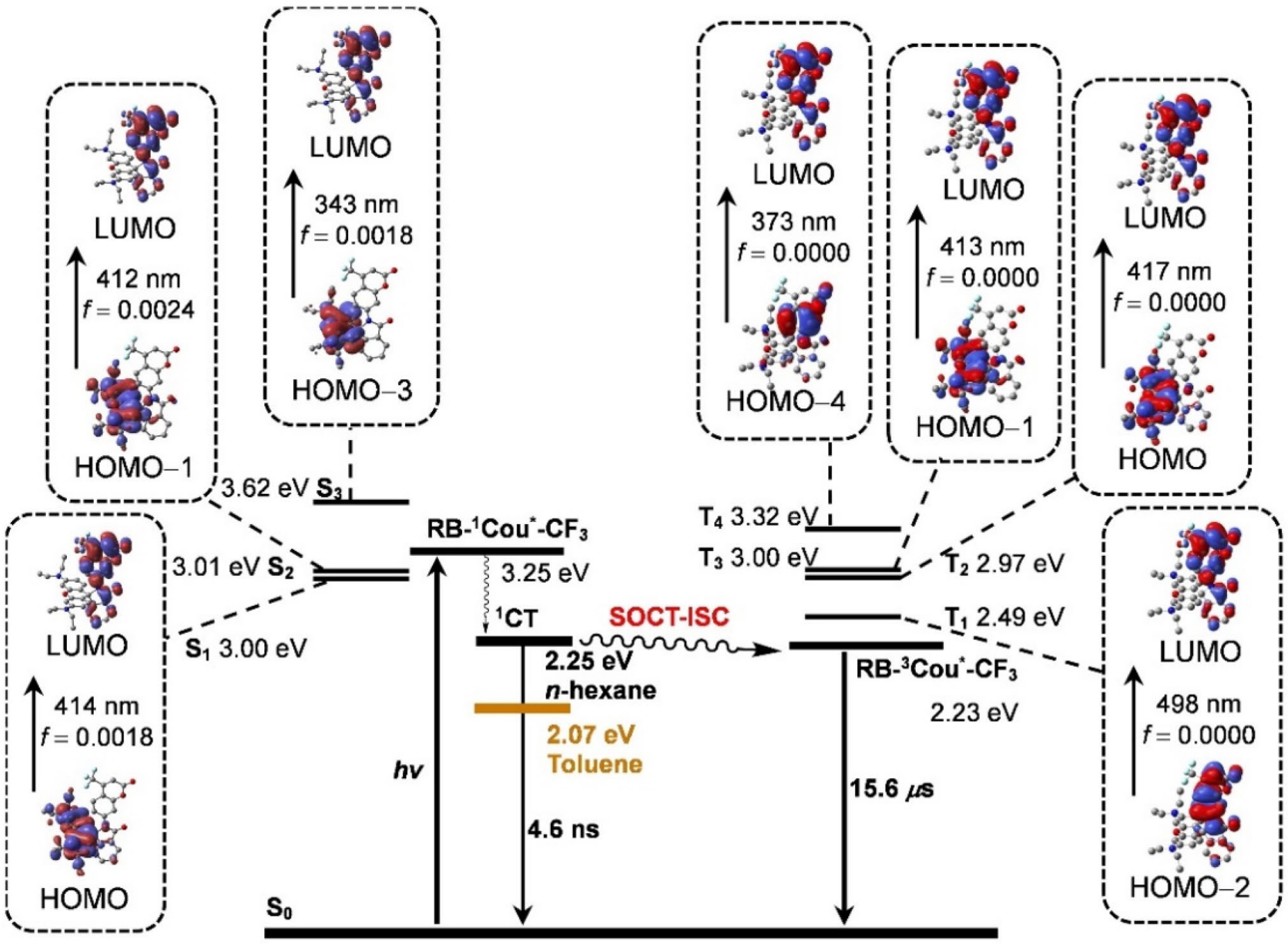

Scheme 2 Simplified Jablonski diagram illustrating the photophysical processes involved in the **RB-Cou-CF$_3$: RB-^{1}Cou*-CF$_3$** energy level is obtained from the crossing point of the normalized UV–vis absorption and fluorescence emission spectra, in *n*-hexane. ^{1}CT energy levels are calculated based on the CT emission band, in *n*-hexane. The lowest triplet excited state (**RB-^{3}Cou*-CF$_3$**) energy was obtained from the phosphorescence at 77 K. The energy of S_n and T_n ($n = 1,2,3,4$) states are also shown with respective transitions, calculated with TDDFT at the B3LYP/6-31G(d) level using Gaussian 09 in vacuum

range-separated functionals i.e. ωB97XD and CAM-B3LYP, similar results were observed (Table S2).

Based on the experimental data and DFT results, the Jablonski diagram was constructed to illustrate the photophysical processes involved in **RB-Cou-CF$_3$** upon photoexcitation (Scheme 2, MOs involved in the transitions are also shown). The occupied molecular orbitals and unoccupied molecular orbitals are localized on rhodamine and coumarin units, respectively. For the calculated S_1, S_2 and S_3 states of the dyad, the corresponding transitions are HOMO → LUMO, HOMO–1 → LUMO and HOMO–3 → LUMO, respectively (Table S3, ESI†). Moreover, for the T_1, T_2, T_3 and T_4 states, the corresponding transitions are HOMO–2 → LUMO, HOMO → LUMO, HOMO–1 → LUMO and HOMO–4 → LUMO. In addition, the T_1 and T_4 states exhibit ^{3}LE feature, which indicates that T_1 and T_4 states of dyads are localized on the coumarin unit. However, the T_2 and T_3 states are with CT features and lie significantly above the ^{3}LE state.

We assume that both the dyads can undergo SO-ISC (S_1 to the near T_n state and through internal conversion (IC) to form T_1) or SOCT-ISC to generate the ^{3}Cou* state (localized on coumarin moiety). However, singlet oxygen quantum yields and CT emission bands (observed in *n*-hexane) indicate that the formation of ^{3}Cou* state in the dyads is not based on SO–ISC mechanism. Hence, SOCT-ISC mechanism is the only way to form the triplet state in these dyads. Upon photoexcitation, ^{1}Cou* state is first populated subsequently charge separation takes place and leads to populating ^{1}CT state. Herein, there are two optional paths for charge recombination (CR). One is directly decayed to the ground state (with CT emission lifetimes of 4.6 ns for **RB-Cou-CF$_3$**), and another relaxation path is SOCT-ISC to populate the ^{3}Cou* state. We observed a coumarin localized triplet

state via SOCT-ISC mechanism with a lifetime of 15.6 µs. A similar energy diagram was constructed to demonstrate the photophysical processes of **RB-Cou-CN** (Scheme S1, ESI†).

4 Conclusion

In summary, we prepared *spiro* rhodamine (RB)-coumarin (Cou) compact electron donor–acceptor dyads, in which the lactam form of the rhodamine unit is the electron donor and the cyano- or trifluoromethyl substituted coumarin as the electron acceptor (**RB-Cou-CF$_3$** and **RB-Cou-CN**), as well as the visible light-harvesting chromophore. The aim of designing such a novel molecular structural motif is to study the spin–orbit charge transfer intersystem crossing (SOCT-ISC) mechanism. CT emission bands were observed for **RB-Cou-CF$_3$** (at 550 nm) and **RB-Cou-CN** (at 595 nm), although there is no significant electronic interaction between electron donor and acceptor at the ground state. Based on the phosphorescence of the dyads observed at 77 K in frozen solution, the energy of the coumarin-localized triplet state of the dyads was determined (2.17 eV for **RB-Cou-CN** and 2.23 eV for **RB-Cou-CF$_3$**). The shallow potential energy curves of the dyads against the torsion of the linkers indicate that the flexible molecular conformation may contribute to the insufficient SOCT-ISC efficiency and the low singlet oxygen quantum yields ($\Phi_\Delta = 3.2–7.5\%$). By maintaining the geometry constrain between donor and acceptor as orthogonal dihedral range and ^{1}CT-^{3}LE energy matching could improve the SOCT-ISC efficiency. According to the DFT/TDDFT calculations, electrochemical study and nanosecond transient absorption (ns-TA) spectral data, ^{3}Cou* state is formed only in non-polar solvent via SOCT-ISC, the triplet states lifetimes are 15.6 µs (**RB-Cou-CF$_3$**) and 11.0 µs (**RB-Cou-CN**). In polar solvents such as acetonitrile, no ^{3}Cou* state was observed in the ns-TA spectra, because of the low-lying CT states (ca. 1.90 eV). Thus, the proposed photophysical path for RB-Cou compact D-A dyads is as follows: RB-^{1}Cou* → RB$^{+\bullet}$-Cou$^{-\bullet}$ → RB-^{3}Cou*. Our studies are useful for the design of compact electron donor/acceptor dyads showing spin–orbit charge transfer intersystem crossing (SOCT-ISC) and for the formation of long-lived triplet states.

Supplementary Information The online version contains supplementary material available at https://doi.org/10.1007/s43630-022-00285-1.

Acknowledgements We thank the NSFC (U2001222, 21761142005 and 21911530095) and the State Key Laboratory of Fine Chemicals for financial support.

Declarations

Conflict of interests There are no conflicts to declare.

References

1. Kamkaew, A., Lim, S. H., Lee, H. B., Kiew, L. V., Chung, L. Y., & Burgess, K. (2013). Bodipy dyes in photodynamic therapy. *Chemical Society Reviews, 42*, 77–88. https://doi.org/10.1039/C2CS35216H
2. Zhao, J., Wu, W., Sun, J., & Guo, S. (2013). Triplet photosensitizers: From molecular design to applications. *Chemical Society Reviews, 42*, 5323–5351. https://doi.org/10.1039/C3CS35531D
3. Zhao, J., Xu, K., Yang, W., Wang, Z., & Zhong, F. (2015). The triplet excited state of bodipy: Formation, modulation and application. *Chemical Society Reviews, 44*, 8904–8939. https://doi.org/10.1039/C5CS00364D
4. Prier, C. K., Rankic, D. A., & MacMillan, D. W. C. (2013). Visible light photoredox catalysis with transition metal complexes: Applications in organic synthesis. *Chemical Reviews, 113*, 5322–5363. https://doi.org/10.1021/cr300503r
5. Hari, D. P., & König, B. (2014). Synthetic applications of eosin Y in photoredox catalysis. *Chemical Communications, 50*, 6688–6699. https://doi.org/10.1039/C4CC00751D
6. Shi, L., & Xia, W. (2012). Photoredox functionalization of C-H bonds adjacent to a nitrogen tom. *Chemical Society Reviews, 41*, 7687–7697. https://doi.org/10.1039/C2CS35203F
7. Tian, J., Zhou, J., Shen, Z., Ding, L., Yu, J.-S., & Ju, H. (2015). A ph-activatable and aniline-substituted photosensitizer for near-infrared cancer theranostics. *Chemical Science, 6*, 5969–5977. https://doi.org/10.1039/C5SC01721A
8. Nguyen, V.-N., Qi, S., Kim, S., Kwon, N., Kim, G., Yim, Y., Park, S., & Yoon, J. (2019). An emerging molecular design approach to heavy-atom-free photosensitizers for enhanced photodynamic therapy under hypoxia. *Journal of the American Chemical Society, 141*, 16243–16248. https://doi.org/10.1021/jacs.9b09220
9. Stacey, O. J., & Pope, S. J. A. (2013). New avenues in the design and potential application of metal complexes for photodynamic therapy. *RSC Advances, 3*, 25550–25564. https://doi.org/10.1039/C3RA45219K
10. Xu, C.-H., Sun, W., Zhang, C., Zhou, C., Fang, C.-J., & Yan, C.-H. (2009). Luminescence switching of a cyclometalated iridium(III) complex through a redox-active tetrathiafulvalene-based ligand. *Chemistry—A European Journal*, *15,* 8717–8721. https://doi.org/10.1002/chem.200901483.
11. Fernández-Moreira, V., Thorp-Greenwood, F. L., & Coogan, M. P. (2010). Application of d6 transition metal complexes in fluorescence cell imaging. *Chemical Communications, 46*, 186–202. https://doi.org/10.1039/B917757D
12. Feng, Y., Cheng, J., Zhou, L., Zhou, X., & Xiang, H. (2012). Ratiometric optical oxygen sensing: A review in respect of material design. *The Analyst, 137*, 4885–4901. https://doi.org/10.1039/C2AN35907C
13. Dai, F.-R., Zhan, H.-M., Liu, Q., Fu, Y.-Y., Li, J.-H., Wang, Q.-W., Xie, Z., Wang, L., Yan, F., & Wong, W.-Y. (2012). Platinum(II)–bis(aryleneethynylene) complexes for solution-processible molecular bulk heterojunction solar cells. *Chemistry—A European Journal*, *18,* 1502–1511. https://doi.org/10.1002/chem.201102598.
14. Singh-Rachford, T. N., & Castellano, F. N. (2010). Photon upconversion based on sensitized triplet–triplet annihilation. *Coordination Chemistry Reviews, 254*, 2560–2573. https://doi.org/10.1016/j.ccr.2010.01.003
15. Zhao, J., Ji, S., & Guo, H. (2011). Triplet–triplet annihilation based upconversion: From triplet sensitizers and triplet acceptors to upconversion quantum yields. *RSC Advances, 1*, 937–950. https://doi.org/10.1039/C1RA00469G
16. Monguzzi, A., Tubino, R., Hoseinkhani, S., Campione, M., & Meinardi, F. (2012). Low power, non-coherent sensitized photon up-conversion: Modelling and perspectives. *Physical Chemistry*

Chemical Physics, 14, 4322–4332. https://doi.org/10.1039/C2CP23900K
17. Simon, Y. C., Weder, C. (2012). Low-power photon upconversion through triplet–triplet annihilation in polymers. *Journal of Materials Chemistry*, *22,* 20817–20830. https://doi.org/10.1039/C2JM33654E.
18. N. J. Turro, V. R., J. C. Scaiano. (2009). Principles of molecular photochemistry: An introduction; University Science Books: Sausalito, California.
19. Bröring, M., Krüger, R., Link, S., Kleeberg, C., Köhler, S., Xie, X., Ventura, B., & Flamigni, L. (2008). Bis(BF2)-2,2'-bidipyrrins (BisBODIPYs): highly fluorescent bodipy dimers with large stokes shifts. *Chemistry—A European Journal*, *14*, 2976–2983. https://doi.org/10.1002/chem.200701912.
20. Ventura, B., Marconi, G., Bröring, M., Krüger, R., & Flamigni, L. (2009). Bis(BF_2)-2,2'-bidipyrrins, a class of bodipy dyes with new spectroscopic and photophysical properties. *New Journal of Chemistry, 33*, 428–438. https://doi.org/10.1039/B813638F
21. Ziessel, R., Allen, B. D., Rewinska, D. B., & Harriman, A. (2009). Selective triplet-state formation during charge recombination in a fullerene/bodipy molecular dyad (bodipy = boron-dipyrromethene). *Chemistry—A European Journal*, 15, 7382–7393. https://doi.org/10.1002/chem.200900440.
22. Wu, W., Zhao, J., Sun, J., & Guo, S. (2012). Light-harvesting fullerene dyads as organic triplet photosensitizers for triplet–triplet annihilation upconversions. *The Journal of Organic Chemistry, 77*, 5305–5312. https://doi.org/10.1021/jo300613g
23. Huang, L., Yu, X., Wu, W., & Zhao, J. (2012). Styryl bodipy-C_{60} dyads as efficient heavy-atom-free organic triplet photosensitizers. *Organic Letters, 14*, 2594–2597. https://doi.org/10.1021/ol3008843
24. Liu, Y., & Zhao, J. (2012). Visible light-harvesting perylenebisimide–fullerene (c_{60}) dyads with bidirectional "ping-pong" energy transfer as triplet photosensitizers for photooxidation of 1,5-dihydroxynaphthalene. *Chemical Communications, 48*, 3751–3753. https://doi.org/10.1039/C2CC30345K
25. Wang, Z., Zhao, J., Barbon, A., Toffoletti, A., Liu, Y., An, Y., Xu, L., Karatay, A., Yaglioglu, H. G., Yildiz, E. A., et al. (2017). Radical-enhanced intersystem crossing in new bodipy derivatives and application for efficient triplet–triplet annihilation upconversion. *Journal of the American Chemical Society, 139*, 7831–7842. https://doi.org/10.1021/jacs.7b02063
26. Wang, Z., Gao, Y., Hussain, M., Kundu, S., Rane, V., Hayvali, M., Yildiz, E. A., Zhao, J., Yaglioglu, H. G., & Das, R., et al. (2018). Efficient radical-enhanced intersystem crossing in an NDI-TEMPO dyad: photophysics, electron spin polarization, and application in photodynamic therapy. *Chemistry—A European Journal*, *24,* 18663–18675. https://doi.org/10.1002/chem.201804212.
27. Smith, M. B., & Michl, J. (2010). Singlet fission. *Chemical Reviews, 110*, 6891–6936. https://doi.org/10.1021/cr1002613
28. Kasha, M., Rawls, H. R., & EI-Bayoumi, M. A. (1965). The exciton model in molecular spectroscopy. *Pure and Applied Chemistry, 11*, 371–392.
29. Gibbons, D. J., Farawar, A., Mazzella, P., Leroy-Lhez, S., & Williams, R. M. (2020). Making triplets from photo-generated charges: Observations, mechanisms and theory. *Photochemical & Photobiological Sciences, 19*, 136–158. https://doi.org/10.1039/C9PP00399A
30. Filatov, M. A. (2020). Heavy-atom-free bodipy photosensitizers with intersystem crossing mediated by intramolecular photoinduced electron transfer. *Organic & Biomolecular Chemistry, 18*, 10–27. https://doi.org/10.1039/C9OB02170A
31. Hou, Y., Zhang, X., Chen, K., Liu, D., Wang, Z., Liu, Q., Zhao, J., & Barbon, A. (2019). Charge separation, charge recombination, long-lived charge transfer state formation and intersystem crossing in organic electron donor/acceptor dyads. *Journal of Materials Chemistry C, 7*, 12048–12074. https://doi.org/10.1039/C9TC04285G
32. Levanon, H., Norris, J. R. (1978). The photoexcited triplet state and photosynthesis. *Chemical Reviews 78,* 185–198. https://doi.org/10.1021/cr60313a001.
33. Guldi, D. M. (2000). Fullerenes: Three dimensional electron acceptor materials. *Chemical Communications*. https://doi.org/10.1039/A907807J
34. Kc, C. B., Lim, G. N., Nesterov, V. N., Karr, P. A., & D'Souza, F. (2014). Phenothiazine–bodipy–fullerene triads as photosynthetic reaction center models: Substitution and solvent polarity effects on photoinduced charge separation and recombination. *Chemistry—A European Journal*, *20,* 17100–17112. https://doi.org/10.1002/chem.201404863.
35. Verhoeven, J. W. (2006). On the role of spin correlation in the formation, decay, and detection of long-lived, intramolecular charge-transfer states. *Journal of Photochemistry and Photobiology C: Photochemistry Reviews, 7*, 40–60. https://doi.org/10.1016/j.jphotochemrev.2006.04.001
36. Dance, Z. E. X., Mi, Q., McCamant, D. W., Ahrens, M. J., Ratner, M. A., & Wasielewski, M. R. (2006). Time-resolved epr studies of photogenerated radical ion pairs separated by p-phenylene oligomers and of triplet states resulting from charge recombination. *The Journal of Physical Chemistry B, 110*, 25163–25173. https://doi.org/10.1021/jp063690n
37. Chen, K.-Y., Hsieh, C.-C., Cheng, Y.-M., Lai, C.-H., Chou, P.-T., & Chow, T. J. (2006). Tuning excited-state electron transfer from an adiabatic to nonadiabatic type in donor−bridge−acceptor systems and the associated energy-transfer process. *The Journal of Physical Chemistry A, 110*, 12136–12144. https://doi.org/10.1021/jp063038s
38. Colvin, M. T., Ricks, A. B., Scott, A. M., Co, D. T., & Wasielewski, M. R. (2012). Intersystem crossing involving strongly spin exchange-coupled radical ion pairs in donor–bridge–acceptor molecules. *The Journal of Physical Chemistry A, 116*, 1923–1930. https://doi.org/10.1021/jp212546w
39. Filatov, M. A., Karuthedath, S., Polestshuk, P. M., Savoie, H., Flanagan, K. J., Sy, C., Elisabeth, S., Telitchko, M., Laquai, F., Boyle, R. W., et al. (2017). Generation of triplet excited states via photoinduced electron transfer in meso-anthra-bodipy: Fluorogenic response toward singlet oxygen in solution and in vitro. *Journal of the American Chemical Society, 139*, 6282–6285. https://doi.org/10.1021/jacs.7b00551
40. Hu, W., Liu, M., Zhang, X.-F., Wang, Y., Wang, Y., Lan, H., & Zhao, H. (2019). Can bodipy-electron acceptor conjugates act as heavy atom-free excited triplet state and singlet oxygen photosensitizers via photoinduced charge separation-charge recombination mechanism? *The Journal of Physical Chemistry C, 123*, 15944–15955. https://doi.org/10.1021/acs.jpcc.9b02961
41. Filatov, M. A., Karuthedath, S., Polestshuk, P. M., Callaghan, S., Flanagan, K. J., Telitchko, M., Wiesner, T., Laquai, F., & Senge, M. O. (2018). Control of triplet state generation in heavy atom-free bodipy–anthracene dyads by media polarity and structural factors. *Physical Chemistry Chemical Physics, 20*, 8016–8031. https://doi.org/10.1039/C7CP08472B
42. Callaghan, S., Filatov, M. A., Savoie, H., Boyle, R. W., & Senge, M. O. (2019). In vitro cytotoxicity of a library of bodipy-anthracene and -pyrene dyads for application in photodynamic therapy. *Photochemical & Photobiological Sciences, 18*, 495–504. https://doi.org/10.1039/C8PP00402A
43. Filatov, M. A., Karuthedath, S., Polestshuk, P. M., Callaghan, S., Flanagan, K. J., Wiesner, T., Laquai, F., & Senge, M. O. (2018). Bodipy-pyrene and perylene dyads as heavy-atom-free singlet oxygen sensitizers. *ChemPhotoChem, 2*, 606–615. https://doi.org/10.1002/cptc.201800020

44. Weiss, E. A., Ahrens, M. J., Sinks, L. E., Ratner, M. A., & Wasielewski, M. R. (2004). Solvent control of spin-dependent charge recombination mechanisms within donor−conjugated bridge−acceptor molecules. *Journal of the American Chemical Society, 126*, 9510–9511. https://doi.org/10.1021/ja047205i
45. Buck, J. T., Boudreau, A. M., DeCarmine, A., Wilson, R. W., Hampsey, J., & Mani, T. (2019). Spin-allowed transitions control the formation of triplet excited states in orthogonal donor-acceptor dyads. *Chem, 5*, 138–155. https://doi.org/10.1016/j.chempr.2018.10.001
46. Hou, Y., Biskup, T., Rein, S., Wang, Z., Bussotti, L., Russo, N., Foggi, P., Zhao, J., Di Donato, M., Mazzone, G., et al. (2018). Spin–orbit charge recombination intersystem crossing in phenothiazine–anthracene compact dyads: Effect of molecular conformation on electronic coupling, electronic transitions, and electron spin polarizations of the triplet states. *The Journal of Physical Chemistry C, 122*, 27850–27865. https://doi.org/10.1021/acs.jpcc.8b08965
47. Wang, Z., & Zhao, J. (2017). Bodipy–anthracene dyads as triplet photosensitizers: Effect of chromophore orientation on triplet-state formation efficiency and application in triplet–triplet annihilation upconversion. *Organic Letters, 19*, 4492–4495. https://doi.org/10.1021/acs.orglett.7b02047
48. Chen, K., Yang, W., Wang, Z., Iagatti, A., Bussotti, L., Foggi, P., Ji, W., Zhao, J., & Di Donato, M. (2017). Triplet excited state of bodipy accessed by charge recombination and its application in triplet–triplet annihilation upconversion. *The Journal of Physical Chemistry A, 121*, 7550–7564. https://doi.org/10.1021/acs.jpca.7b07623
49. Imran, M., Sukhanov, A. A., Wang, Z., Karatay, A., Zhao, J., Mahmood, Z., Elmali, A., Voronkova, V. K., Hayvali, M., Xing, Y. H., et al. (2019). Electronic coupling and spin–orbit charge-transfer intersystem crossing in phenothiazine–perylene compact electron donor/acceptor dyads. *The Journal of Physical Chemistry C, 123*, 7010–7024. https://doi.org/10.1021/acs.jpcc.8b12040
50. Rehmat, N., Toffoletti, A., Mahmood, Z., Zhang, X., Zhao, J., & Barbon, A. (2020). Carbazole-perylenebisimide electron donor/acceptor dyads showing efficient spin orbit charge transfer intersystem crossing (SOCT-ISC) and photo-driven intermolecular electron transfer. *Journal of Materials Chemistry C, 8*, 4701–4712. https://doi.org/10.1039/C9TC06429J
51. Zhao, Y., Sukhanov, A. A., Duan, R., Elmali, A., Hou, Y., Zhao, J., Gurzadyan, G. G., Karatay, A., Voronkova, V. K., & Li, C. (2019). Study of the spin–orbit charge transfer intersystem crossing of perylenemonoimide–phenothiazine compact electron donor/acceptor dyads with steady-state and time-resolved optical and magnetic spectroscopies. *The Journal of Physical Chemistry C, 123*, 18270–18282. https://doi.org/10.1021/acs.jpcc.9b04896
52. Zhao, Y., Duan, R., Zhao, J., & Li, C. (2018). Spin–orbit charge transfer intersystem crossing in perylenemonoimide–phenothiazine compact electron donor–acceptor dyads. *Chemical Communications, 54*, 12329–12332. https://doi.org/10.1039/C8CC07012A
53. Tang, G., Sukhanov, A. A., Zhao, J., Yang, W., Wang, Z., Liu, Q., Voronkova, V. K., Di Donato, M., Escudero, D., & Jacquemin, D. (2019). Red thermally activated delayed fluorescence and the intersystem crossing mechanisms in compact naphthalimide–phenothiazine electron donor/acceptor dyads. *The Journal of Physical Chemistry C, 123*, 30171–30186. https://doi.org/10.1021/acs.jpcc.9b09335
54. Liu, D., El-Zohry, A. M., Taddei, M., Matt, C., Bussotti, L., Wang, Z., Zhao, J., Mohammed, O. F., Di Donato, M., & Weber, S. (2020). Long-lived charge-transfer state induced by spin-orbit charge transfer intersystem crossing (SOCT-ISC) in a compact spiro electron donor/acceptor dyad. *Angewandte Chemie International Edition, 59*, 11591–11599. https://doi.org/10.1002/anie.202003560
55. Qi, Q., Huang, L., Yang, R., Li, J., Qiao, Q., Xu, B., Tian, W., Liu, X., & Xu, Z. (2019). Rhodamine-naphthalimide demonstrated a distinct aggregation-induced emission mechanism: Elimination of dark-states via dimer interactions (EDDI). *Chemical Communications, 55*, 1446–1449. https://doi.org/10.1039/C8CC09212E
56. Çamur, M., Bulut, M., Özkaya, A. R., Kandaz, M., & Yaylı, N. (2007). Coumarin-derivatized fluorescent vic-dioxime-type ligand and its complexes; the preparation, spectroscopy, and electrochemistry. *Transition Metal Chemistry, 32*, 642–648. https://doi.org/10.1007/s11243-007-0220-8
57. Priyadarsini, K. I., Naik, D. B., & Moorthy, P. N. (1989). Triplet state of coumarin 153 studied by nanosecond pulse radiolysis. *Journal of Photochemistry and Photobiology A: Chemistry, 46*, 239–246. https://doi.org/10.1016/1010-6030(89)80010-3
58. Montalti, M., Credi, A., Prodi, L., & Gandolfi, M. T. (2006). *Handbook of Photochemistry*. CRC Press.
59. Murakami, M., Ohkubo, K., Nanjo, T., Souma, K., Suzuki, N., & Fukuzumi, S. (2010). Photoinduced electron transfer in photorobust coumarins linked with electron donors affording long lifetimes of triplet charge-separated states. *ChemPhysChem, 11*, 2594–2605. https://doi.org/10.1002/cphc.201000096
60. Liu, B., Wang, R., Mi, W., Li, X., & Yu, H. (2012). Novel branched coumarin dyes for dye-sensitized solar cells: Significant improvement in photovoltaic performance by simple structure modification. *Journal of Materials Chemistry, 22*, 15379–15387. https://doi.org/10.1039/C2JM32333H
61. Wu, Y., & Zhu, W. (2013). Organic sensitizers from D–π–A to D-A–π–A: Effect of the internal electron-withdrawing units on molecular absorption, energy levels and photovoltaic performances. *Chemical Society Reviews, 42*, 2039–2058. https://doi.org/10.1039/C2CS35346F
62. Tyson, D. S., & Castellano, F. N. (1999). Light-harvesting arrays with coumarin donors and MLCT acceptors. *Inorganic Chemistry, 38*, 4382–4383. https://doi.org/10.1021/ic9905300
63. Ji, S., Guo, H., Wu, W., Wu, W., & Zhao, J. (2011). Ruthenium(II) polyimine–coumarin dyad with non-emissive ^{3}IL excited state as sensitizer for triplet–triplet annihilation based upconversion. *Angewandte Chemie International Edition, 50*, 8283–8286. https://doi.org/10.1002/anie.201008134
64. Yi, X., Zhao, J., Wu, W., Huang, D., Ji, S., & Sun, J. (2012). Rhenium(I) tricarbonyl polypyridine complexes showing strong absorption of visible light and long-lived triplet excited states as a triplet photosensitizer for triplet–triplet annihilation upconversion. *Dalton Transactions, 41*, 8931–8940. https://doi.org/10.1039/C2DT30804E
65. Frisch, M. J., Trucks, G. W., Schlegel, H. B., Scuseria, G. E., Robb, M. A., Cheeseman, J. R., Montgomery, J. J. A., Vreven, T., Kudin, K. N., & Burant, J. C. et al. Gaussian 09w, *Revision E.01*; Wallingford, CT, 2009.
66. Lee, M. H., Han, J. H., Lee, J. H., Park, N., Kumar, R., Kang, C., & Kim, J. S. (2013). Two-color probe to monitor a wide range of PH values in cells. *Angewandte Chemie International Edition, 52*, 6206–6209. https://doi.org/10.1002/anie.201301894
67. Hu, M., Sukhanov, A. A., Zhang, X., Elmali, A., Zhao, J., Ji, S., Karatay, A., & Voronkova, V. K. (2021). Spiro rhodamine-perylene compact electron donor–acceptor dyads: Conformation restriction, charge separation, and spin–orbit charge transfer intersystem crossing. *The Journal of Physical Chemistry B, 125*, 4187–4203. https://doi.org/10.1021/acs.jpcb.1c02071
68. Anglos, D., Bindra, V., & Kuki, A. (1994). Photoinduced electron transfer and long-lived charge separation in rigid peptide architectures. *Journal of the Chemical Society, Chemical Communications*. https://doi.org/10.1039/C39940000213
69. Sun, Q., Li, J., Liu, W.-N., Dong, Q.-J., Yang, W.-C., & Yang, G.-F. (2013). Non-peptide-based fluorogenic small-molecule

probe for elastase. *Analytical Chemistry, 85*, 11304–11311. https://doi.org/10.1021/ac402097g
70. Takakura, H., Sasakura, K., Ueno, T., Urano, Y., Terai, T., Hanaoka, K., Tsuboi, T., & Nagano, T. (2010). Development of luciferin analogues bearing an amino group and their application as BRET donors. *Chemistry—An Asian Journal*, *5,* 2053–2061. https://doi.org/10.1002/asia.201000219.
71. Beaulieu, P. L., Anderson, P. C., Bethell, R., Bös, M., Bousquet, Y., Brochu, C., Cordingley, M. G., Fazal, G., Garneau, M., Gillard, J. R., et al. (2014). Discovery of BI 207524, an indole diamide NS5B thumb pocket 1 inhibitor with improved potency for the potential treatment of chronic hepatitis C virus infection. *Journal of Medicinal Chemistry, 57*, 10130–10143. https://doi.org/10.1021/jm501532z
72. Hay, M. P., Atwell, G. J., Wilson, W. R., Pullen, S. M., & Denny, W. A. (2003). Structure−activity relationships for 4-nitrobenzyl carbamates of 5-aminobenz[e]indoline minor groove alkylating agents as prodrugs for gdept in conjunction with E. Coli nitroreductase. *Journal of Medicinal Chemistry, 46*, 2456–2466. https://doi.org/10.1021/jm0205191
73. De, P. (2004). Efficient reductions of nitroarenes with $SnCl_2$ in ionic liquid. *Synlett, 2004*(10), 1835–1837.
74. K, N., K, V., G, P. (2017). A simple and one step commercially cost effective process for eluxadoline intermediates. *Journal of Chemical and Pharmaceutical Research, 9*, 256–258.
75. Sasaki, S., Hattori, K., Igawa, K., & Konishi, G.-I. (2015). Directional control of π-conjugation enabled by distortion of the donor plane in diarylaminoanthracenes: A photophysical study. *The Journal of Physical Chemistry A, 119*, 4898–4906. https://doi.org/10.1021/acs.jpca.5b03238
76. Catalán, J. (2013). On the dual emission of p-dimethylaminobenzonitrile and its photophysical implications. *Physical Chemistry Chemical Physics, 15*, 8811–8820. https://doi.org/10.1039/C3CP44627A
77. Valeur, B., & Berberan-Santos, M. (2012). *Molecular Fluorescence: Principles and Applications*. Wiley-VCH.
78. Shi, W.-J., El-Khouly, M. E., Ohkubo, K., Fukuzumi, S., Ng, D. K. P. (2013). Photosynthetic antenna-reaction center mimicry with a covalently linked monostyryl boron-dipyrromethene–aza-boron-dipyrromethene–C_{60} triad. *Chemistry—A European Journal*, *19,* 11332–11341. https://doi.org/10.1002/chem.201300318.
79. Suneesh, C. V., & Gopidas, K. R. (2010). Long-lived photoinduced charge separation due to the inverted region effect in 1,6-bis(phenylethynyl)pyrene−phenothiazine dyad. *The Journal of Physical Chemistry C, 114*, 18725–18734. https://doi.org/10.1021/jp107606t
80. Huang, D., Sun, J., Ma, L., Zhang, C., & Zhao, J. (2013). Preparation of ketocoumarins as heavy atom-free triplet photosensitizers for triplet–triplet annihilation upconversion. *Photochemical & Photobiological Sciences, 12*, 872–882. https://doi.org/10.1039/C3PP25416J
81. Yi, X., Zhang, C., Guo, S., Ma, J., & Zhao, J. (2014). Strongly emissive long-lived ^{3}IL excited state of coumarins in cyclometalated Ir(III) complexes used as triplet photosensitizers and application in triplet–triplet annihilation upconversion. *Dalton Transactions, 43*, 1672–1683. https://doi.org/10.1039/C3DT52306C
82. Sun, H., Guo, H., Wu, W., Liu, X., & Zhao, J. (2011). Coumarin phosphorescence observed with N-N Pt(II) bisacetylide complex and its applications for luminescent oxygen sensing and triplet–triplet-annihilation based upconversion. *Dalton Transactions., 2011*(40), 7834–7841. https://doi.org/10.1039/C1DT10490J
83. Wang, Z., Sukhanov, A. A., Toffoletti, A., Sadiq, F., Zhao, J., Barbon, A., Voronkova, V. K., & Dick, B. (2019). Insights into the efficient intersystem crossing of bodipy-anthracene compact dyads with steady-state and time-resolved optical/magnetic spectroscopies and observation of the delayed fluorescence. *The Journal of Physical Chemistry C, 123*, 265–274. https://doi.org/10.1021/acs.jpcc.8b10835